JACS
JOURNAL OF THE AMERICAN CHEMICAL SOCIETY
Article
pubs.acs.org/JACS

Rate-Enhancing Roles of Water Molecules in Methyltrioxorhenium-Catalyzed Olefin Epoxidation by Hydrogen Peroxide

Bryan R. Goldsmith,[†,#] Taeho Hwang,[†,#] Stefan Seritan,[‡] Baron Peters,*[,†,‡] and Susannah L. Scott*[,†,‡]

[†]Department of Chemical Engineering, University of California, Santa Barbara, California 93106-5080, United States
[‡]Department of Chemistry and Biochemistry, University of California, Santa Barbara, California 93106-9510, United States

Supporting Information

ABSTRACT: Olefin epoxidation catalyzed by methyltrioxorhenium (MTO, CH_3ReO_3) is strongly accelerated in the presence of H_2O. The participation of H_2O in each of the elementary steps of the catalytic cycle, involving the formation of the peroxo complexes ($CH_3ReO_2(\eta^2\text{-}O_2)$, **A**, and $CH_3ReO(\eta^2\text{-}O_2)_2(H_2O)$, **B**), as well as in their subsequent epoxidation of cyclohexene, was examined in aqueous acetonitrile. Experimental measurements demonstrate that the epoxidation steps exhibit only weak [H_2O] dependence, attributed by DFT calculations to hydrogen bonding between uncoordinated H_2O and a peroxo ligand. The primary cause of the observed H_2O acceleration is the strong co-catalytic effect of water on the rates at which **A** and **B** are regenerated and consequently on the relative abundances of the three interconverting Re-containing species at steady state. Proton transfer from weakly coordinated H_2O_2 to the oxo ligands of MTO and **A**, resulting in peroxo complex formation, is directly mediated by solvent H_2O molecules. Computed activation parameters and kinetic isotope effects, in combination with proton-inventory experiments, suggest a proton shuttle involving one or (most favorably) two H_2O molecules in the key ligand-exchange steps to form **A** and **B** from MTO and **A**, respectively.

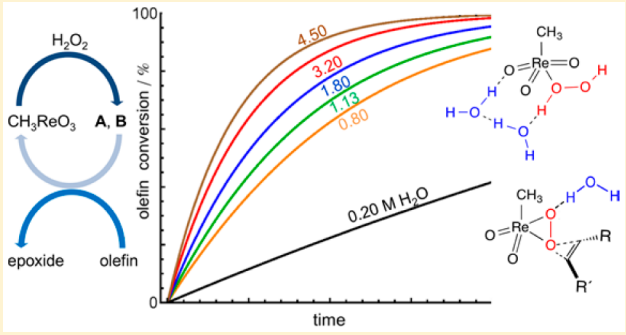

INTRODUCTION

Epoxidation reactions are important in the manufacturing of consumer and pharmaceutical products, including polyurethane plastics, resins, adhesives, and excipients for tablet binding. CH_3ReO_3 (MTO) is particularly efficient as a homogeneous catalyst for the epoxidation of a wide variety of olefins using H_2O_2, at room temperature and below.[1−4] In contrast to many other catalysts, MTO produces epoxides with near-quantitative selectivity, without catalyzing H_2O_2 disproportionation.[5] In the catalytic cycle, MTO undergoes sequential and reversible ligand exchange with H_2O_2, forming the mono- and bis(peroxo) complexes **A** and **B**, commonly depicted as shown in Scheme 1.[5−7] Both **A** and **B** are kinetically competent intermediates, co-existing with MTO in the presence of H_2O_2, resulting in two coupled catalytic cycles whose relative contributions to the epoxidation rate depend on the reaction conditions.[7,8] Interestingly, although neither peroxo complex formation nor the olefin epoxidation steps require H_2O as a reactant explicitly,[7,9,10] the rate of epoxidation has been noted to depend strongly on the water content of the solvent system.[5,11]

Interest in catalytic reactions that can be performed in and "on" water[12] is growing because of environmental concerns about the use of organic solvents and the ubiquitousness of water in reactions involving biomass-derived chemicals.[13,14] Dramatic reaction-rate enhancements have been attributed to strong hydrophobic effects that promote reactant assemblies, transition-state stabilization due to solute−solvent hydrogen bonding, and/or the ability of water to act as a proton shuttle.[12,15,16] Water is known to be critical in CO oxidation over Au/TiO_2,[17,18] methanol-to-gasoline production over zeolites,[19] and $Ru(X)(Y)(PMe_3)_4$-catalyzed hydrogenation of CO_2.[20] There is mounting evidence for acceleration of olefin epoxidation by hydrogen bonding for both transition-metal catalysts[21−24] and metal-free catalysts[25,26] and in epoxide ring-opening.[27] Yet the precise mechanistic role of water is often poorly understood. In the case of homogeneous MTO-catalyzed oxidations, a detailed understanding of the water dependence is complicated by the reversibility of peroxo ligand exchange, differences in the hydration states of the Re-

Scheme 1. Sequential, Reversible Reactions of MTO with H_2O_2 As Reported[5−7,10] To Yield the mono- and bis(Peroxo) Complexes A and B, Which Epoxidize Olefins at Similar Rates

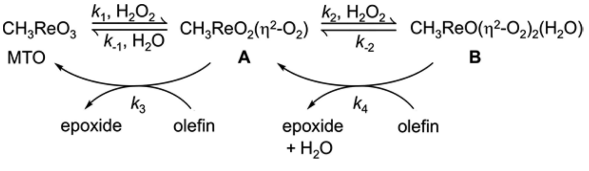

Received: April 10, 2015
Published: July 2, 2015

DOI: 10.1021/jacs.5b03750
J. Am. Chem. Soc. 2015, 137, 9604−9616

containing intermediates, and the strong non-ideality of semiaqueous solutions.[28−30]

The reported water sensitivity of overall olefin epoxidation rates could be caused by differential solvation effects, direct involvement of H_2O in either the epoxidation steps or the catalyst activation steps (i.e., the formation of **A** and **B** from MTO and H_2O_2) or some combination of these. Although the behavior of the MTO/H_2O_2/olefin system has been the subject of many prior reports, its remarkable water dependence has yet to be explained. In most prior studies, the solvent composition was held constant to avoid complicating the kinetic analysis, even though this practice inevitably obscures any direct role of the solvent in the reaction.[2,7,8,10] Pestovsky et al. initially suggested a direct ligand-exchange mechanism for the formation of **A** and **B** from MTO and H_2O_2,[31] and structures for the corresponding intermediates were computed by Gonzales et al.[32] Yet Wang and Espenson reported that both k_1 and k_2 are ca. 100 times faster in neat H_2O relative to CH_3CN containing 2.6 M H_2O, and they hypothesized an explicit role for water in the ligand-exchange mechanism.[33]

In principle, computational analysis can aid in elucidating the role of solvent molecules in complex reactions, and omitting the solvent can lead to dramatically incorrect predictions whose discrepancies are far higher than accepted errors in modern DFT methods.[34] However, accurate computational descriptions of solvent participation are still challenging. One approach is to combine ab initio MD and QM/MM methods with importance sampling methods, but such studies are typically limited to single elementary steps.[35−37] In addition, involving explicit solvent molecules in a reaction mechanism requires sampling of ensembles of microsolvated states.[38,39] These approaches are not yet practical for multistep reaction networks. Implicit solvent contributions are more easily analyzed in such networks, but the limited accuracy typically restricts their use to describing qualitative trends.[40−42] Consequently, most previous computational studies of MTO were limited to unsolvated species[43,44] or, at best, reactions in the presence of a solvent continuum.[32,45,46] Recently, Kuznetsov and Pombeiro computed favorable ligand-exchange transition states involving a single, explicit water molecule, although without comparison to experimental observables.[45] In our recent computational study, we reported that including one explicit water molecule in each ligand-exchange transition state narrows the gap between observed and calculated kinetics by several orders of magnitude.[34] However, the agreement was still not satisfactory, and we speculated that our initial description of solvent participation was incomplete.

In this contribution, we use a combination of experimental kinetic measurements and DFT calculated transition states, as well as kinetic simulations, to explore the participation of water in olefin epoxidation catalyzed by MTO. Namely, we address: (i) the relative magnitudes of the rate enhancements due to water, in the epoxide formation steps vs the peroxide activation steps; (ii) the relative importance of water-catalyzed and uncatalyzed pathways; (iii) the roles and precise numbers of water molecules involved in each step of the epoxidation catalytic cycle; and (iv) the extent to which DFT calculations, despite limitations in chemical accuracy, can predict and explain the observed kinetics of the complex solution-phase reaction involving multiple proton transfers, via modeling of specific transition states and ensemble averaging. The kinetically important role of water as a co-catalyst in MTO-catalyzed epoxidations has implications for attempts to conduct such reactions under low-water conditions,[10,47,48] which may be desirable in order to slow subsequent epoxide hydrolysis.

EXPERIMENTAL METHODS

Materials. CH_3ReO_3 (MTO, Aldrich), CH_3CN (HPLC grade, Fisher), CD_3CN (99.8%, Cambridge Isotope Laboratories, Inc.), D_2O (99.9%, Cambridge Isotope Laboratories, Inc.), $HClO_4$ (70 wt%, Aldrich), and cyclohexene (99%, Aldrich) were used as received. H_2O_2 (30 wt% aqueous solution, EMS Chemicals) was diluted with deionized water and standardized by iodometric titration.

Kinetic Measurements Using ^{1}H NMR Spectroscopy. The kinetics of the reaction between cyclohexene and H_2O_2, catalyzed by MTO in aqueous CD_3CN, were investigated by recording ^{1}H NMR spectra on an Avance DMX500 NMR spectrometer. The minimum water concentration is limited by $[H_2O_2]$, since this reagent was used as an aqueous solution. The initial MTO and H_2O_2 concentrations were fixed at 4.0 mM and 200 mM, respectively, while the initial concentration of H_2O was varied. Decomposition of peroxorhenium complexes (to form CH_3OH and CH_3OOH) was suppressed by adding 0.100 M $HClO_4$.[8,33] To study the kinetics under $[H_2O_2]$-limited conditions, cyclohexene (2.0 M) was added last, to initiate the reaction after equilibria involving the peroxo complexes were established. The temperature was maintained at 15.0 °C, to minimize subsequent (noncatalytic) diol formation via epoxide hydrolysis.[47,49] $CHCl_3$ (2.0 M) was added as an internal standard to quantify the reaction products. Reaction progress was monitored via the change in intensity of the signal for the olefinic protons of cyclohexene (5.64 ppm); using other reactant/product signals gave very similar results. The fractional conversion, X, is defined in eq 1:

$$X = \frac{[\text{olefin}]_0 - [\text{olefin}]}{[R]_0} \tag{1}$$

where $[\text{olefin}]_0$ is the initial olefin concentration, [olefin] is the remaining concentration of olefin, and $[R]_0$ is the initial concentration of the limiting reagent (cyclohexene or H_2O_2).

To study the kinetics under [olefin]-limited conditions, the above procedure was repeated for initial MTO and H_2O_2 concentrations of 2.0 mM and 500 mM, respectively, while the initial concentration of H_2O was varied. Cyclohexene (20 mM) was again added last, to initiate the reaction. Note that, unless otherwise stated, all kinetic analyses are based on initial water concentrations, $[H_2O]_0$, since the change in water concentration due to the amounts generated as reaction products is negligible. This is the well-known method of kinetic flooding.

Kinetic Measurements Using UV−vis Spectroscopy. Kinetic profiles were recorded using a Shimadzu UV-2401PC spectrophotometer, equipped with a thermoelectrically temperature-controlled cell holder to maintain constant temperature conditions (±0.1 °C). The absorbance (Abs) was monitored at either 320 or 360 nm, corresponding to λ_{max} for **A** and **B**, respectively.[8,33,34] Rate constants for ligand-exchange reactions involving H_2O_2 were evaluated by nonlinear least-squares curve-fitting of the kinetic profiles using either eq 2 (at 320 nm) or eq 3 (at 360 nm):[34]

$$\text{Abs}_t = \text{Abs}_\infty + \alpha(1 - e^{-k_{\text{fast}}t}) + \beta e^{-k_{\text{slow}}t} \tag{2}$$

$$\text{Abs}_t = \text{Abs}_\infty + \alpha e^{-k_{\text{fast}}t} + \beta e^{-k_{\text{slow}}t} \tag{3}$$

Because the sequential reactions to form **A** and **B** are reversible, the pseudo-first-order rate constants k_{fast} and k_{slow} are combinations of the rate constants for the forward and reverse ligand-exchange reactions, eqs 4 and 5:

$$k_{\text{fast}} + k_{\text{slow}} = (k_1 + k_2)[H_2O_2]_0 + (k_{-1}[H_2O] + k_{-2}) \tag{4}$$

$$k_{\text{fast}}k_{\text{slow}} = k_1k_2[H_2O_2]_0^2 + k_1k_{-2}[H_2O_2]_0 + k_{-1}k_{-2}[H_2O] \tag{5}$$

where $[H_2O_2]_0 \approx [H_2O_2]_{\text{avg}}$, since $[H_2O_2]_0 \gg [\text{Re}]_T$.

Kinetic Simulations. Re speciation was calculated as a function of reaction conditions and reaction progress by numerical analysis, using

DOI: 10.1021/jacs.5b03750
J. Am. Chem. Soc. 2015, 137, 9604−9616

Mathematica 9.0.[50] The analysis is based on Scheme 1, from which the following coupled equations are obtained:

$$\frac{d[\mathbf{A}]}{dt} = k_1[\mathrm{MTO}][H_2O_2] + (k_{-2} + k_{4app}[\mathrm{olefin}])[\mathbf{B}] - (k_{-1}[H_2O] + k_2[H_2O_2] + k_{3app}[\mathrm{olefin}])[\mathbf{A}] \quad (6)$$

$$\frac{d[\mathbf{B}]}{dt} = k_2[H_2O_2][\mathbf{A}] - (k_{-2} + k_{4app}[\mathrm{olefin}])[\mathbf{B}] \quad (7)$$

$$\frac{d[\mathrm{epoxide}]}{dt} = (k_{3app}[\mathbf{A}] + k_{4app}[\mathbf{B}])[\mathrm{olefin}] \quad (8)$$

$$[H_2O_2] = [H_2O_2]_0 - [\mathbf{A}] - 2[\mathbf{B}] - [\mathrm{epoxide}] \quad (9)$$

$$[\mathrm{Re}]_T = [\mathrm{MTO}] + [\mathbf{A}] + [\mathbf{B}] \quad (10)$$

The equilibrated concentrations of all three Re species (MTO, **A**, and **B**), as well as the concentration of free H_2O_2, were calculated using our previously reported values of $K_1 = k_1/k_{-1}$ and $K_2 = k_2/k_{-2}$.[34] Values of three of the ligand-exchange rate constants (k_1, k_{-1}, k_2) were also obtained from previously reported values measured in CH_3CN containing 2.0 M H_2O at 15.0 °C.[34] Since direct measurement of k_{-2} at 15.0 °C was precluded in that study, k_{-2} values were calculated using activation parameters ($\Delta H_{-2}^{\ddagger}$, $\Delta S_{-2}^{\ddagger}$) measured in the same solvent system.[34] The apparent epoxidation rate constants k_{3app} and k_{4app} were measured at specific water concentrations in this work. The complete solutions for eqs 6−10 were compared to solutions obtained using the pseudo-steady-state approximation[51] for the concentrations of **A** and **B**.

COMPUTATIONAL METHODS

Electronic structure calculations were performed using Gaussian 09.[52] The range-separated ωB97X-D density functional[53] and the aug-def2-TZVP basis sets were used for all atoms, as described previously.[34] We note that even larger basis sets for Re, some of which contain *h*-functions and beyond,[54,55] may further improve accuracy. Transition states were found using the Berny algorithm, as implemented in Gaussian 09. Cartesian coordinates for all species are listed in Table S1; contributions to the total free energy of each species are provided in Tables S2 and S3.

Molecular geometries were optimized in a conductor-type polarizable continuous medium (CPCM).[40,41,56,57] Gaussian 09 CPCM default conditions were used with the solvent specified as CH_3CN and with cavitation, dispersion, and repulsion nonelectrostatic effects included. Computed free energies include CPCM solvation as well as zero-point, translational, rotational, and vibrational contributions obtained from ideal gas partition functions.[58] Entropic contributions to the free energies were computed using the procedure of Kuznetsov and Pombeiro to account for solvation-induced structural correlations.[45] The reference state for all species is 1.0 M, except for H_2O and D_2O, whose concentrations were fixed at 2.0 M for comparison with experiments, unless otherwise noted. A simple explicit microsolvation model[59−62] was constructed to treat water-solute enthalpic interactions consistently during each step of the reaction pathway. A detailed description of our approach is provided in the Supporting Information.

Since multiple transition states, differing in their hydration states, may contribute to the overall rate, the generalized partition function formula in eq 11 was used to compute the free energy for ensembles of transition states.[63]

$$\Delta G_i^{\ddagger} = -k_B T \ln \sum_{x=0}^{n} g_x \exp\left[-\frac{\Delta G_x^{\ddagger}}{k_B T}\right] \quad (11)$$

The ensemble average of transition states *i* contains contributions from transition states containing different numbers of water molecules, *n*, and obeys detailed balance. The factor g_x accounts for the indistinguishability of water molecules in distinct positions of the cyclic transition states. Thus, unassisted and $1H_2O$-assisted transition states have $g_0 = g_1 = 1$, $2H_2O$-assisted transition states have $g_2 = 2$, and $3H_2O$-assisted transition states have $g_3 = 6$. Each term $\Delta G_x^{\ddagger}$ within the summation includes the usual translational, rotational, vibrational, and symmetry free energy contributions. Eq 11 is similarly used to compute free energies for ensembles of intermediate states with varying degrees of hydration.

Rate constants were computed using semiclassical transition-state theory.[64] Tunneling-corrected rate constants, $k = \Gamma(T)\, k_B T/h \exp[-\Delta G_i^{\ddagger}/k_B T]$, were included for all reactions involving proton transfer. The truncated parabolic tunneling correction was chosen, since most tunneling corrections were of order one.[65,66] To include the effect of tunneling in the computed free energies and to allow for direct comparison with experiment, computed values for $\Delta H^{\ddagger}$ and $\Delta S^{\ddagger}$ were not obtained directly from partition functions but were instead extracted from computed Eyring plots to obtain *apparent* activation parameters. This procedure is described in detail in a previous report.[34]

RESULTS AND DISCUSSION

Effect of Water on the Kinetics of Cyclohexene Epoxidation. The solvent dependence of the catalytic epoxidation rate was first studied under $[H_2O_2]$-limited conditions. MTO (4.0 mM) was combined with H_2O_2 (0.20 M) in the presence of variable amounts of H_2O (0.80−1.8 M) in CD_3CN at 15.0 °C, to form an equilibrated mixture dominated by **B** (representing >96% $[\mathrm{Re}]_T$). Epoxidation was initiated by addition of excess cyclohexene (2.0 M), and ^{1}H NMR spectra were recorded until the cyclohexene concentration ceased to change. The resonance for **B** ($\delta \approx 2.8$ ppm, depending on $[H_2O]$) decreased in intensity, being first replaced by **A** ($\delta \approx 2.4$ ppm, depending on $[H_2O]$) and then MTO ($\delta \approx 2.3$ ppm, depending on $[H_2O]$). The sole organic products are the epoxide (90 ± 5%) and the diol (10 ± 5%, formed subsequent to epoxidation by noncatalytic hydrolysis).

Kinetic profiles are shown in Figure 1a. The exponential curvefits demonstrate that the reaction kinetics are approximately pseudo-first-order, eq 12:

$$[\mathrm{epoxide}] = [H_2O_2]_0(1 - \exp[-k_{obs}t]) \quad (12)$$

even with the non-negligible change in $[H_2O]$ at the lowest values of $[H_2O]_0$. The overall epoxidation rate depends strongly on the solvent composition: the inset shows that the fitted values of k_{obs} depend linearly on $[H_2O]_0$. Interestingly, the linear curvefit has a negligible *y*-intercept, suggesting that there is no significant water-independent pathway under these reaction conditions.

Kinetic measurements were also performed under [olefin]-limited conditions. MTO (2.0 mM) was combined with excess H_2O_2 (0.50 M) in the presence of variable amounts of H_2O (3.0−4.5 M) in CD_3CN at 15.0 °C, to form an equilibrated mixture again dominated by **B** (>97% $[\mathrm{Re}]_T$). Epoxidation was initiated by addition of cyclohexene (20 mM). ^{1}H NMR spectra

DOI: 10.1021/jacs.5b03750
J. Am. Chem. Soc. 2015, 137, 9604−9616

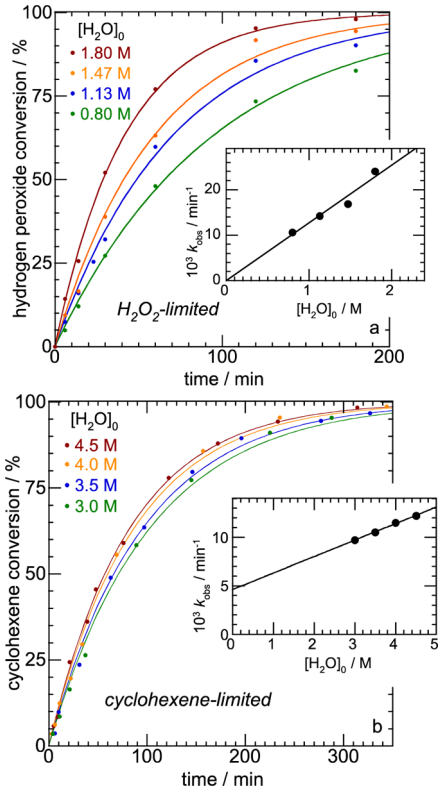

Figure 1. Water dependence of the rate of cyclohexene epoxidation by MTO/H_2O_2, in time-resolved conversion profiles (points) measured by ^{1}H NMR at 15.0 °C in aqueous CD_3CN. (a) Under [H_2O_2]-limited conditions: 2.0 M cyclohexene, 0.20 M H_2O_2, 4.0 mM MTO, variable amounts of H_2O (0.80−1.8 M). Inset: Water dependence of the pseudo-first-order rate constants. (b) Under [olefin]-limited conditions: 20 mM cyclohexene, 0.50 M H_2O_2, 2.0 mM MTO, variable amounts of H_2O (3.0−4.5 M). Inset: Water dependence of the pseudo-first-order rate constants. The curvefits (lines) were obtained using the integrated first-order rate equation with one adjustable parameter (k_{obs}).

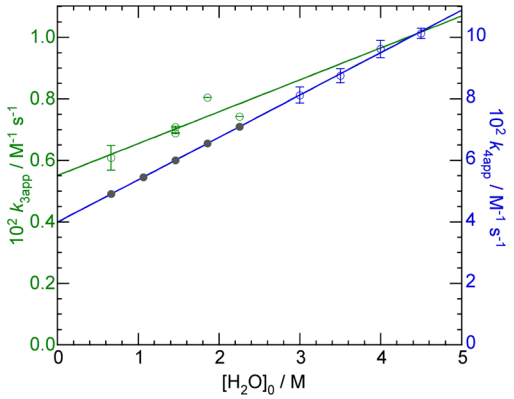

Figure 2. Water dependence of the second-order rate constants k_{3app} (green) and k_{4app} (blue) for the epoxidation of cyclohexene by **A** and **B**, respectively, at 15.0 °C. Values of k_{4app} at lower water concentrations (solid gray points) were extrapolated from eq 14 and used in the biexponential fits shown in Figure 3, in which the corresponding values of k_{3app} were refined.

were recorded until the cyclohexene was completely converted. Throughout the reaction, the intensity of the resonance for **B** remained constant and much larger than the signals for either **A** or MTO. Kinetic profiles recorded with excess H_2O_2 and the corresponding exponential curvefits are shown in Figure 1b. The rate depends on [olefin] and $[Re]_T$ but is independent of [H_2O_2],[9] eq 13:

$$[\text{epoxide}] = [\text{olefin}]_0(1 - \exp[-k_{obs}t]) \quad (13)$$

For these experiments, we note that $[H_2O]_0 \approx [H_2O]_{avg}$ for all values of $[H_2O]_0$. Thus, since nearly all Re is present as **B** (and small amounts of **A** generated during the reaction make little contribution to the rate), the curvefits reflect k_{4app} directly, with $k_{obs} = k_{4app}[Re]_T$.

Despite the limited range of $[H_2O]_0$, the solvent dependence of the rate is clearly weaker under [olefin]-limited conditions compared to [H_2O_2]-limited conditions. The water dependence of k_{4app}, obtained from the k_{obs} values in Figure 1b (inset), is shown in Figure 2 (blue) and described by eq 14:

$$k_{4app} = k_4 + k_{4w}[H_2O]_0 \quad (14)$$

A linear fit to eq 14 yields the water-independent and water-dependent rate constants k_4 and k_{4w}, whose values are (4.0 ± 0.4) × 10^{-2} M^{-1} s^{-1} and (1.38 ± 0.09) × 10^{-2} M^{-2} s^{-1}, respectively, at 15.0 °C.

Direct evaluation of the water dependence of k_{3app} is not possible, since **A** cannot be prepared in pure form; some **B** is always present.[7] However, **A** is the major species responsible for epoxidation when $[Re]_T > [H_2O_2]$. Addition of dilute $HClO_4$ suppresses the spontaneous decomposition of **A** under these conditions, without affecting the rates of either ligand exchange or epoxidation.[8] The addition of 0.50 M cyclohexene to a pre-equilibrated mixture of 10 mM MTO and 2.0 mM H_2O_2 at 15.0 °C was used to initiate epoxidation in the presence of variable amounts of H_2O (0.67−2.25 M). The initial Re speciation, [MTO]:[**A**]:[**B**], is calculated to be 8.8:1.1:0.12, based on integration of the ^{1}H NMR signals. Using rate constants obtained from experimental $\Delta G^{\ddagger}$ values (Tables 1 and 2, *vide infra*), we expect the rate of reaction of **A** with cyclohexene to be ca. 2 orders of magnitude faster than the rate of reaction of **A** with H_2O_2 to form **B**. Thus, the kinetic profiles primarily reflect the epoxidation rate, which is dominated here by the reaction of **A** with cyclohexene.

The reaction progress was monitored using UV−vis spectroscopy to record the conversion of **A** + **B**, as shown in Figure 3. For the rate law shown in eq 8, biexponential curvefits were obtained with k_{4app} values fixed at the values extrapolated using eq 14 for each water concentration. The resulting values of k_{3app}, shown in Figure 2 (green), are described by eq 15:

$$k_{3app} = k_3 + k_{3w}[H_2O]_0 \quad (15)$$

A linear fit to eq 15 yields the water-independent and water-dependent rate constants k_3 and k_{3w}, whose values are (5.3 ± 0.6) × 10^{-3} M^{-1} s^{-1} and (1.14 ± 0.39) × 10^{-3} M^{-2} s^{-1}, respectively, at 15.0 °C. Figure 2 shows that the pseudo-second-order rate constants k_{3app} and k_{4app} have (i) similar magnitudes, with $k_{4app} \approx 10\ k_{3app}$ for a given [H_2O]; and (ii) similar, weak water dependences.

Water Acceleration of Peroxo Complex Formation. The very small changes in epoxidation rate constants with water concentration suggest that most of the observed water acceleration arises not in the epoxidation steps but in the catalyst regeneration steps, i.e., the ligand-exchange reactions with H_2O_2. To explore the precise role of water in these reactions, the kinetics of the reaction between MTO and H_2O_2

DOI: 10.1021/jacs.5b03750
J. Am. Chem. Soc. 2015, 137, 9604−9616

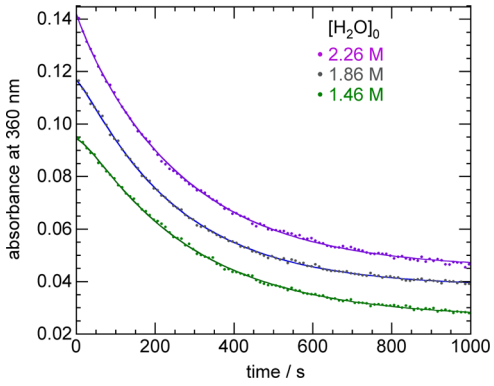

Figure 3. UV−vis kinetic profiles (points) recorded during the epoxidation of 0.50 M cyclohexene by a mixture of **A** (1.1 mM) and **B** (0.12 mM), formed by the reaction of 10 mM MTO with 2.0 mM H_2O_2 in the presence of 0.100 M $HClO_4$ and variable amounts of water, in CH_3CN at 15.0 °C. The curvefits (lines) are biexponential. Curves are vertically offset for clarity.

were measured in CH_3CN at 25.0 °C in the presence of varying amounts of water, up to 4.0 M. The absorbance−time profiles recorded at 320 and 360 nm, shown in Figure 4, are strongly

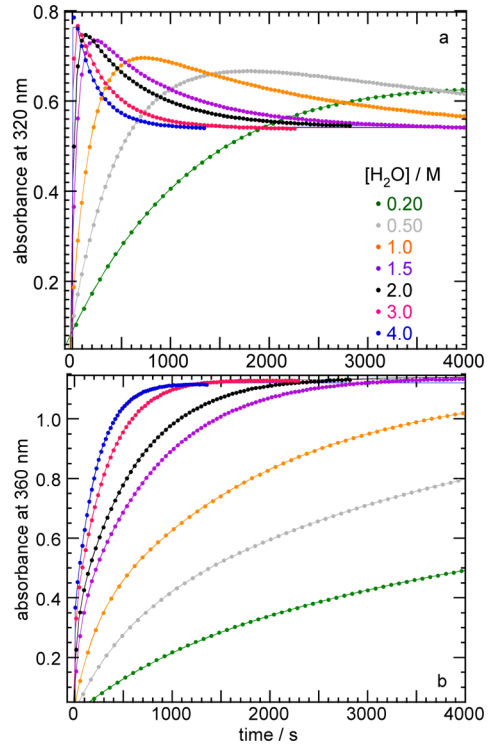

Figure 4. Time-resolved UV−vis kinetic profiles (points), recorded at two wavelengths: (a) 320 nm and (b) 360 nm, for the reaction of 1.0 mM MTO with 49.1 mM H_2O_2, in the presence of variable amounts of H_2O (0.20−4.0 M) in CH_3CN at 25.0 °C. The curvefits (lines) were obtained using eqs 2 and 3.

water dependent. Curvefits to the biexponential kinetic equations in eqs 2 and 3 were used to obtain values for k_{fast} and k_{slow}. The results are shown in Figure 5, expressed as the sum and product of the pseudo-first-order rate constants (as required to extract values of the $[H_2O_2]$-independent rate constants via eqs 4 and 5).[34,67] Figure 5 reveals that the acceleration by water is slightly greater for k_{fast} (dominated by

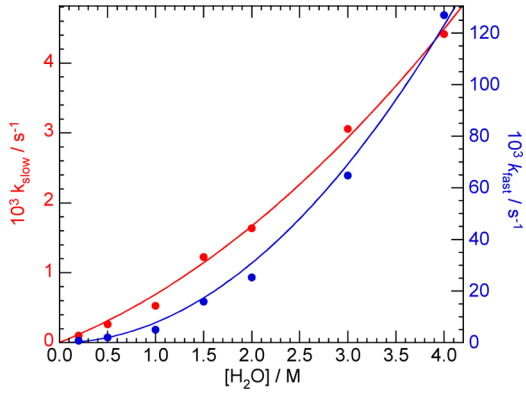

Figure 5. Water dependence of the measured pseudo-first-order rate constants k_{fast} (blue points) and k_{slow} (red points) for the reaction of 1.0 mM MTO with 49.1 mM H_2O_2, in aqueous CH_3CN at 25.0 °C. The curvefits (lines) correspond to a second-order dependence on $[H_2O]$ (for k_{fast}), and a mixed first- and second-order dependence on $[H_2O]$ (for k_{slow}).

k_1) than for k_{slow} (dominated by k_2), with the former showing approximately second-order dependence and the latter showing approximately mixed first- and second-order dependence on $[H_2O]$.

A detailed description of the water dependence of the experimental rate law for peroxo complex formation is complicated by the reversibility of formation of **A** and **B** and differences in the $[H_2O]$ reaction orders for the reverse reactions, as required by detailed balance and their different hydration states. Nevertheless, Figure 5 suggests that the rate-determining transition states for both ligand-exchange reactions involve 1−2 water molecules. However, the dependence of the rate constants on $[H_2O]$ may not yield an accurate value for the orders with respect to H_2O, due to the strong non-ideality of water−acetonitrile mixtures.[30,68,69] Kinetic analyses in which water activity is used to determine reaction orders often report complicated, nonpower law dependences. For example, the hydrolysis of (*p*-methylphenyl)trichloroacetate in aqueous acetonitrile was described with a reaction order with respect to water of (3.1 ± 0.1) at low $[H_2O]$ and (9.9 ± 0.1) at high $[H_2O]$.[70] Such complicated water dependence may reflect changes in the microstructure of the water−acetonitrile mixture, including the formation of microheterogeneous water-rich clusters.[28,30,71]

Quantitative Assessment of Water Participation. The proton inventory technique was used to ascertain the number of water molecules participating directly in each ligand-exchange transition state.[70,72,73] In this technique, the kinetic consequences of partial isotopic labeling of the solvent are assessed to determine the number of protons transferred in the rate-determining step.[70,72,74] Since the total water concentration is held constant, while the solvent H/D ratio is varied, non-ideality of the solvent system does not complicate the analysis.

The Gross−Butler equation[70,73,75] relates the rate constant k_n measured for a given D atom fraction, n, to the rate constant k_0 when H_2O is the only isotopolog present. If we assume that each participating water molecule has the same fractionation factor and further that the fractionation factors of H_2O and H_2O_2 are similar (since both form O−H−O hydrogen bonds in the transition states), the Gross−Butler equation can be written as eq 16:

DOI: 10.1021/jacs.5b03750
J. Am. Chem. Soc. 2015, 137, 9604−9616

$$k_n/k_0 = (1 - n + n\phi^*_{H_2O_2})(1 - n + n\phi^*_{H_2O})^m$$
$$= (1 - n + n\phi^*)^{m+1} \quad (16)$$

where m is the number of water molecules involved in the rate-determining transition state and ϕ^* represents the isotope fractionation factor for the H/D-exchangeable site that participates directly in the transition state. The form of the exponent $(m+1)$ arises because ligand-exchange reactions with H_2O_2 necessarily involve the transfer of at least one proton (i.e., from H_2O_2 itself) in the rate-determining transition state. A detailed explanation of the procedure to obtain eq 16 is given in the Supporting Information.

The solvent kinetic isotope effect (KIE) was evaluated experimentally for the reaction between MTO and H_2O_2 in CH_3CN containing 3.1 M (H_2O + D_2O). Since proton exchange between H_2O_2 and H_2O is rapid, the contribution of H_2O_2 to the deuterium atom fraction must be included, i.e., n = $[D_2O]/([H_2O + D_2O] + [H_2O_2])$. Kinetic profiles, recorded by UV−vis spectroscopy at 25.0 °C, were analyzed as described above for Figure 4. As expected, both pseudo-first-order rate constants k_{fast} and k_{slow} decrease with increasing n. To extract the pseudo-second-order rate constants k_1 and k_2, $[H_2O_2]$ was varied to give the results shown in Figure 6.

Values for $(k_1 + k_2)$ and $(k_1 \times k_2)$ were obtained from the curvefits to eqs 4 and 5, then values of k_1 and k_2 were extracted for each deuterium atom fraction. The dependence of k_1 and k_2 on n is presented in Figure 7. The close similarity of the two data sets suggests that the same number of water molecules is

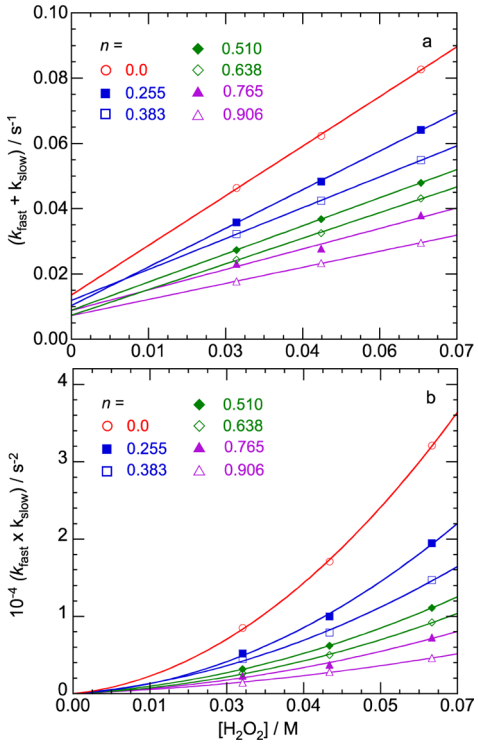

Figure 6. Dependence on excess $[H_2O_2]$ of (a) the sum of the observed rate constants $(k_{fast} + k_{slow})$, showing curvefits obtained using eq 4; and (b) the product of the observed rate constants $(k_{fast} \times k_{slow})$, showing curvefits obtained using eq 5, at seven different H_2O/D_2O ratios, expressed as the atom fraction of deuterium, n, for the reaction of 1.0 mM MTO in CH_3CN containing with 3.1 M (H_2O+D_2O), at 25.0 °C.

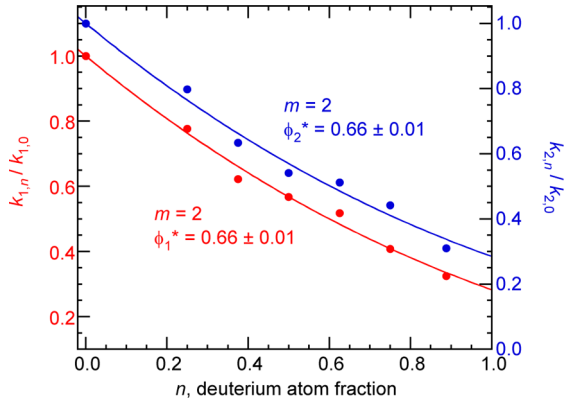

Figure 7. Dependence of the normalized pseudo-second-order rate constants $k_{1,n}/k_{1,0}$ (red) and $k_{2,n}/k_{2,0}$ (blue) on the solvent deuterium atom fraction (n) for the reaction of MTO with H_2O_2, in CH_3CN containing 3.1 M (H_2O + D_2O), at 25.0 °C. The best curvefits (lines) were obtained using eq 16 with m = 2 and one adjustable parameter, ϕ_i^* (R^2 = 0.9905 for k_1, and 0.9840 for k_2).

involved in the rate-determining step for each ligand-exchange reaction, i.e., conversion of MTO to **A** (ϕ_1^*) and of **A** to **B** (ϕ_2^*). The data were analyzed using eq 16, for different integer values of m representing the number of water protons participating in the transition state. The best fits, corresponding to m = 2, are shown in Figure 7 (inferior curvefits obtained for m = 0 and 1 are compared in Figure S1). Thus, we infer that each rate-determining transition state involves on average two H_2O molecules (although the experiments do not exclude a role for transition states with one or three water molecules, depending on $[H_2O]$). Our finding of m = 2 is generally consistent with the nonlinearity observed in Figure 5.

The fitted values of the fractionation factors, ϕ_1^* = (0.656 ± 0.009) and ϕ_2^* = (0.658 ± 0.011), represent the average fractionation factors for the three protons (representing one from H_2O_2, and one from each of two H_2O molecules) transferred in each reaction coordinate. Their magnitudes agree well with other values for reactions with three-proton transition states. For example, fractionation factors of (0.697 ± 0.005) and (0.707 ± 0.003) were reported for the hydrolysis of (*p*-nitrophenyl)trifluoroacetate[76] and (*p*-methylphenyl)-trifluoroacetate,[70] respectively, in aqueous acetonitrile. The corresponding transition states were assumed to involve proton transfer from H_2O mediated by two additional H_2O molecules via a hydrogen-bond wire.[77] In the sequential reactions of MTO with H_2O_2, we infer that two free water molecules and (necessarily) one coordinated H_2O_2 molecule form hydrogen-bonded eight-membered rings, Figure 8. These transition states lead to the η^1-hydroperoxo intermediates $\mathbf{I_1}$ and $\mathbf{I_2}$. While these intermediates have never been observed, they are assumed to convert to **A** and **B** in rapid subsequent proton transfer steps.[34]

The conclusions which can be drawn regarding the participation of water in catalytic olefin epoxidation based on the kinetic experiments described above are summarized in Scheme 2. Both peroxo binding rate constants k_{1w} and k_{2w} are fourth-order rate constants, with values of 0.106 and 0.0069 M^{-3} s^{-1}, respectively, at 25.0 °C. The water dependence of the reverse rate constants k_{-1} and k_{-2} was not measured experimentally but is required by detailed balance. For further insight into the mechanistic role of water in both the peroxide activation and olefin epoxidation steps, we turned to computational modeling.

DOI: 10.1021/jacs.5b03750
J. Am. Chem. Soc. 2015, 137, 9604−9616

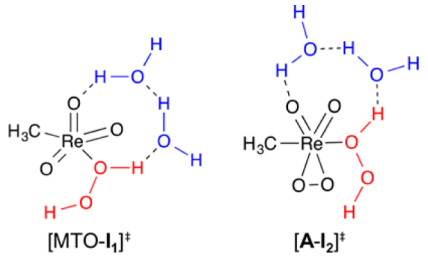

Figure 8. Proposed cyclic transition states associated with proton transfer via a hydrogen-bond wire during ligand exchange to form the mono(η^1-hydroperoxo) intermediate $\mathbf{I_1}$ and the bis(η^1-hydroperoxo) intermediate $\mathbf{I_2}$.

Scheme 2. Water Involvement in Cyclohexene Epoxidation Catalyzed by MTO, As Required by Kinetic Experiments

1. Ligand exchange/peroxide activation:

$$\underset{\mathbf{MTO}}{CH_3ReO_3} + H_2O_2 + 2\,H_2O \underset{k_{-1w}}{\overset{k_{1w}}{\rightleftharpoons}} \underset{\mathbf{A}}{CH_3ReO_2(\eta^2\text{-}O_2)} + 3\,H_2O$$

$$\underset{\mathbf{A}}{CH_3ReO_2(\eta^2\text{-}O_2)} + H_2O_2 + 2\,H_2O \underset{k_{-2w}}{\overset{k_{2w}}{\rightleftharpoons}} \underset{\mathbf{B}}{CH_3ReO(\eta^2\text{-}O_2)_2(H_2O)} + 2\,H_2O$$

2. Olefin epoxidation:

$$\underset{\mathbf{A}}{CH_3ReO_2(\eta^2\text{-}O_2)} + \bigcirc \xrightarrow{k_3} \underset{\mathbf{MTO}}{CH_3ReO_3} + \bigcirc\!O$$

$$\underset{\mathbf{A}}{CH_3ReO_2(\eta^2\text{-}O_2)} + H_2O + \bigcirc \xrightarrow{k_{3w}} \underset{\mathbf{MTO}}{CH_3ReO_3} + H_2O + \bigcirc\!O$$

$$\underset{\mathbf{B}}{CH_3ReO(\eta^2\text{-}O_2)_2(H_2O)} + \bigcirc \xrightarrow{k_4} \underset{\mathbf{A}}{CH_3ReO_2(\eta^2\text{-}O_2)} + H_2O + \bigcirc\!O$$

$$\underset{\mathbf{B}}{CH_3ReO(\eta^2\text{-}O_2)_2(H_2O)} + H_2O + \bigcirc \xrightarrow{k_{4w}} \underset{\mathbf{A}}{CH_3ReO_2(\eta^2\text{-}O_2)} + 2\,H_2O + \bigcirc\!O$$

Computational Modeling of Water Participation in Cyclohexene Epoxidation. In aqueous acetonitrile near ambient temperature, **A** does not bind water, while **B** does.[78] However, the structures of **A** and **A·H$_2$O**, and of **B** and its water-free analog **B′**, differ only slightly in free energy.[34] Consequently, their interconversion eqs 17 and 18 could potentially contribute to the water dependence of the epoxidation kinetics:

$$\underset{\mathbf{A}(\text{major})}{CH_3ReO_2(\eta^2\text{-}O_2)} + H_2O \rightleftarrows \underset{\mathbf{A\cdot H_2O}(\text{minor})}{CH_3ReO_2(\eta^2\text{-}O_2)(H_2O)} \quad (17)$$

$$\underset{\mathbf{B}(\text{major})}{CH_3ReO(\eta^2\text{-}O_2)_2H_2O} \rightleftarrows \underset{\mathbf{B}'(\text{minor})}{CH_3ReO(\eta^2\text{-}O_2)_2} + H_2O \quad (18)$$

For example, water acceleration for k_{3app} would result if both **A** and the minor species $CH_3ReO_2(\eta^2\text{-}O_2)(H_2O)$ (i.e., **A·H$_2$O**) contribute to the observed epoxidation rate, and **A·H$_2$O** is the more reactive of the two equilibrated species. However, the similar water dependence observed for k_{4app} cannot arise from the kinetic competence of the minor species $CH_3ReO(\eta^2\text{-}O_2)_2$ (i.e., **B′**), because the water-free complex is the minor species in this equilibrium. It is also possible that water accelerates the epoxidation reactions by interacting with **A** and **B** without directly bonding to Re, e.g., via hydrogen bonding to the active peroxo ligand.

Each of these possibilities was explored computationally. The free energy barriers for the epoxidation of cyclohexene by **A** and **B**, as well as by the minor species **A·H$_2$O** and **B′**, were computed. In each case, cyclohexene approaches one of the electron-deficient peroxo ligands of **A** or **B**/**B′** in a spiro conformation, i.e., with the electron-rich π-bond perpendicular to the Re(η^2-O$_2$) plane.[79] The peroxo oxygen further from the methyl ligand is the more reactive in O atom transfer.

The water molecule in **A·H$_2$O** does not remain coordinated to **A** during its reaction with cyclohexene; instead, it prefers to hydrogen bond to the nonreacting oxygen of the activated peroxo ligand. The transition state for **A** that includes this hydrogen-bonded water molecule, [**A**-C_6H_{10}-H_2O]‡, is slightly lower in free energy (by 2 kJ mol^{-1}) than the water-free transition state, [**A**-C_6H_{10}]‡. The transition state for **B** (with a coordinated water molecule) reacting with cyclohexene, [**B**-C_6H_{10}]‡, is 3 kJ mol^{-1} lower in free energy than for [**B′**-C_6H_{10}]‡ (i.e., with a water molecule free in solution) at 2 M H_2O. However, an additional water molecule also slightly stabilizes the transition state involving **B** and cyclohexene, [**B**-C_6H_{10}-H_2O]‡ via hydrogen bonding. Computed transition-state geometries are shown in Figure 9.

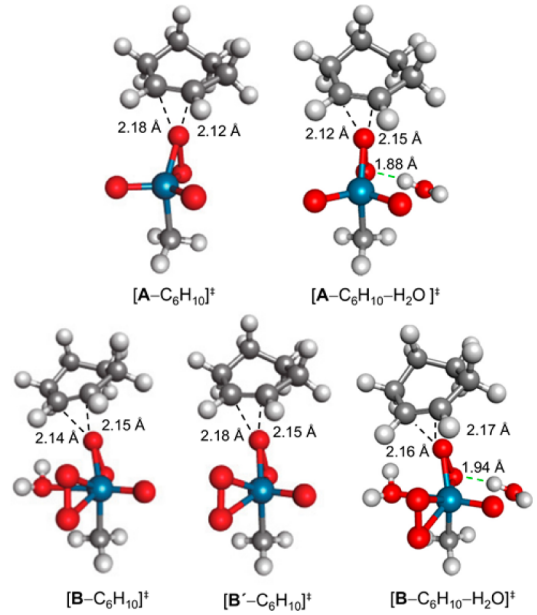

Figure 9. Transition states associated with the MTO-catalyzed epoxidation of cyclohexene by H_2O_2. Color legend: blue, Re; red, O; gray, C; white, H. Green dashed lines indicate hydrogen bonding. Black dashed lines indicate the trajectory of oxygen atom transfer.

Computed free energy barriers for the epoxidation of cyclohexene by **A**, **B**, and **B′**, with and without an additional hydrogen-bonded water molecule, are compared to experimental values in Table 1. No transition state was located for the epoxidation of cyclohexene by **A·H$_2$O**. In agreement with the experimental trend, we predict **A** to be less reactive than **B**/**B′**. The computed free energy barriers overestimate the experimentally determined values by 22−36 kJ mol^{-1}, similar to the average unsigned electronic energy errors reported for oxygen atom transfers from high-valent Re species using DFT.[80] Nevertheless, the trends are consistent with the weak water dependences of k_{3app} and k_{4app} in Figure 2, predicting small rate accelerations for increasing water concentrations via water stabilization of the transition states through hydrogen bonding ([**A**-C_6H_{10}-H_2O]‡ and [**B**-C_6H_{10}-H_2O]‡).

Computational Modeling of Water Participation in the Reactions between MTO and H_2O_2. Free energy

DOI: 10.1021/jacs.5b03750
J. Am. Chem. Soc. 2015, 137, 9604−9616

Table 1. Comparison of Experimental and Computed Free Energy Barriers $\Delta G^{\ddagger}$ (kJ mol^{-1}) for Cyclohexene Epoxidation in Aqueous Acetonitrile at 15.0 °C for Various Water Concentrations

	exp.[a]	calculated[b]		
		[H_2O]/M		
transition-state description	2	2	4	8
A + C_6H_{10} → [**A**-C_6H_{10}]‡	82	118	118	118
A + C_6H_{10} + H_2O → [**A**-C_6H_{10}-H_2O]‡		116	115	114
B + C_6H_{10} → [**B**-C_6H_{10}]‡	77	96	96	96
B + C_6H_{10} → [**B**′-C_6H_{10}]‡ + H_2O		99	100	102
B + C_6H_{10} + H_2O → [**B**-C_6H_{10}-H_2O]‡		97	96	94

[a]Harmonic transition-state theory was applied to the measured epoxidation rate constants (extrapolated using eqs 14 and 15) to estimate the experimental free energy barriers at 15.0 °C and 2.0 M H_2O. [b]Free energies are for standard concentrations (1.0 M) of all reactants except for water, whose concentration varies as indicated.

barriers for the peroxo ligand-exchange reactions were computed for four reaction pathways: one involving direct proton transfer (unassisted), and three involving explicit water molecules that participate directly in the transition states (water-assisted). We assume there is an ensemble of stable complexes having varying degrees of association with H_2O, according to their relative free energies. Likewise, we assume an ensemble of transition states having varying degrees of H_2O participation according to the relative free energies of the transition states. The possible transition states are designated $0H_2O$, $1H_2O$, $2H_2O$, and $3H_2O$, to indicate states involving zero, one, two, and three water molecules.

Transition states containing zero, one, two, and three water molecules consist of four-, six-, eight-, and 10-membered rings, respectively (Table S1). For water chains containing one or two H_2O molecules, proton transfer via a hydrogen-bond wire[77] was verified computationally by examining the intrinsic reaction coordinate.[81,82] For the rate-determining formation of [MTO-$\mathbf{I}_1$]‡ in the conversion of MTO to **A** and for the rate-determining formation of [**A**-$\mathbf{I}_2$]‡ in the conversion of **A** to **B**, the free energy barriers are comparable for transition states containing either one or two H_2O molecules, Figure 10. However, the nonrate-determining steps, involving proton transfer in the η^1-hydroperoxo transition states ([$\mathbf{I}_1$-**A**]‡ and [$\mathbf{I}_2$-**B**]‡), are computed to be fastest when they include just one H_2O.

We also computed $3H_2O$-assisted transition states, in which four protons are transferred via a 10-membered ring. In contrast to the $1H_2O$- and $2H_2O$-assisted transition states, the intrinsic reaction coordinates do not show concerted proton transfer along the hydrogen bond wire. Instead, an H_3O^+-like intermediate forms. Regardless, we predict $3H_2O$-assisted transition states to be unfavorable due to the large entropic penalty for assembling five molecules in solution, Tables S4 and S5. Consequently, this pathway was neglected in the calculation of the free energy barriers for the ensemble of transition states in Figure 10.

The computed apparent free energies for each mechanism are compared with experimental values in Figure 11. For both the first and second ligand-exchange steps, the free energy barriers are similar for $1H_2O$- and $2H_2O$-assisted transition states, and these are closest to the experimental values. The barriers for the $0H_2O$- and $3H_2O$-assisted transition states are substantially higher. Thus, either one or two water molecules

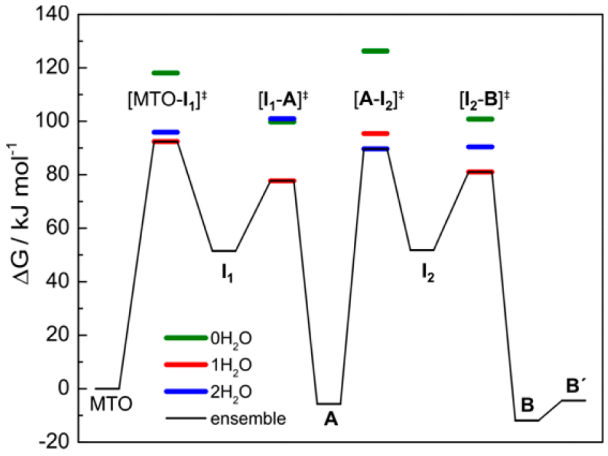

Figure 10. Computed free energies for formation of the peroxo complexes of MTO, including CPCM and entropic corrections for solvation in CH_3CN at 25.0 °C (at a water concentration of 2.0 M, with all other species at 1.0 M; see Table S6 for numerical values). Free energies are presented relative to separated MTO, H_2O_2, and H_2O molecules. Transition states are identified by a hyphen between the reactant and product states of the Re complex. Solid green, red, and blue lines show free energies with $0H_2O$-, $1H_2O$-, and $2H_2O$-assisted transition states. The black solid lines show the free energy profile that includes the ensemble of hydration states for each intermediate and transition state.

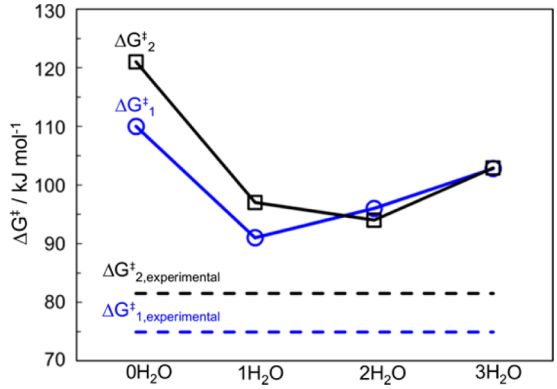

Figure 11. Computed apparent free energy barriers for the formation of the peroxo complexes **A** (blue circles) and **B** (black squares), via transition states involving different numbers of water molecules, compared to experimental values (dashed lines) measured at 25.0 °C with 2.0 M H_2O.

provide optimal transition-state stabilization, and both pathways likely contribute to water-catalyzed ligand-exchange, in proportions that depend on the actual water concentration.

Table 2 shows the computed activation parameters for the unassisted and $1H_2O$- and $2H_2O$-assisted transition states as well as for the ensemble-averaged properties. For each forward and reverse reaction, the computed activation enthalpy decreases as the number of H_2O molecules in the transition state increases, due to favorable hydrogen-bonding interactions. For the reversible formation of **A**, the apparent activation entropy becomes more negative as the number of H_2O molecules in each transition state increases, as expected. However, the trend is more complicated for the reversible formation of **B**. This is due to much more pronounced tunneling in direct (unassisted by water) proton transfer for transition state [**A**-$\mathbf{I}_2$]‡, compared to the water-catalyzed

DOI: 10.1021/jacs.5b03750
J. Am. Chem. Soc. 2015, 137, 9604−9616

Table 2. Comparison between Computed and Experimental Apparent Activation Parameters for H_2O-Catalyzed Pathways in the Formation of Peroxo Complexes A and B[a]

	computed				
parameter	$0H_2O$	$1H_2O$	$2H_2O$	ensemble	experimental[b]
$\Delta G_1^{\ddagger}$	110	91	96	91	74.9
$\Delta G_{-1}^{\ddagger}$	116	95	103	94	89.3
$\Delta G_2^{\ddagger}$	121	97	94	93	81.5
$\Delta G_{-2}^{\ddagger}$	127	106	92	97	93.2
$\Delta H_1^{\ddagger}$	68	43	29	43	8.4
$\Delta H_{-1}^{\ddagger}$	79	50	38	51	20.7
$\Delta H_2^{\ddagger}$	69	46	24	31	19.9
$\Delta H_{-2}^{\ddagger}$	101	82	49	52	52.8
$\Delta S_1^{\ddagger}$	−141	−163	−224	−161	−223
$\Delta S_{-1}^{\ddagger}$	−124	−151	−217	−146	−230
$\Delta S_2^{\ddagger}$	−176	−171	−233	−209	−206
$\Delta S_{-2}^{\ddagger}$	−87	−81	−143	−151	−136

[a]Apparent thermodynamic parameters were computed at 25.0 °C with all species at 1.0 M except for H_2O (2.0 M) and include tunneling corrections. Enthalpies and free energies are reported in kJ mol^{-1}, and entropies in J K^{-1} mol^{-1}. [b]From experiments conducted in CH_3CN containing 2.0 M H_2O at 25.0 °C.[34]

mechanisms (Table S7). The apparent activation entropies for the $2H_2O$-assisted transition states agree strikingly well with experimental values, with absolute deviations of only 1−27 J mol^{-1} K^{-1}. By comparison, the activation entropies are much too positive for both the unassisted and $1H_2O$-assisted transition states; they are much too negative for the $3H_2O$-assisted transition states (Table S4).

Gandour suggested that eight-membered cyclic transition states such as those depicted in Figure 8 should be ideal,[83] since they allow for nearly linear hydrogen bonds (∠OHO = 168.2 ± 5.5° in our computational models). Angles in the six-membered rings formed in the rate-determining steps of the $1H_2O$-assisted transition states are computed to be smaller (∠OHO = 155.1 ± 7.2° in our computational models). Near-linear hydrogen bonding provides strong enthalpic stabilization to the eight-membered ring transition states, compensating for the entropic penalty of assembling four molecules. However, our calculations suggest that six-membered rings are optimum for proton transfer in the nonrate-determining transition states involving reactions of the η^1-hydroperoxo intermediates, suggesting a subtle enthalpic−entropic balance.

The free energy barriers involving both the $1H_2O$- and $2H_2O$-assisted transition states generally agree well with experiment, overpredicting the measured values by only 6−21 kJ mol^{-1} for each step. These errors are within typical ranges for modern density functionals[84−86] (especially for Re(VII) species, which are known to be particularly prone to large errors in electronic energies).[80] The contributions to the enthalpic and entropic barriers for the ensemble averages are dominated by the $1H_2O$- and $2H_2O$-assisted mechanisms. However, the optimum number of water molecules is sensitive to the small differences (ca. 5 kJ mol^{-1}) in $\Delta G^{\ddagger}$ between the $1H_2O$- and $2H_2O$-catalyzed pathways, which are less than DFT accuracy. Although the calculations predict the $1H_2O$-assisted transition states to be slightly favored in the formation of **A** from MTO, changes in the effective water concentration due to non-ideality in the acetonitrile−water mixture (neglected in the calculations due to the absence of information about transition state activities)[87] could easily favor the $2H_2O$-assisted transition states. The generally better agreement with experimental enthalpic and entropic barriers suggests that contributions of the $2H_2O$-assisted transition states dominate under the reaction conditions used here.

Modeling of Kinetic Isotope Effects. In light of the satisfactory agreement between computed and experimental activation parameters, we extended our computational analysis to the KIEs (k_i/k_i^D, where the superscript D denotes a rate constant in D_2O) for each ligand-exchange step, for comparison to the results of the proton inventory experiments described above. Each of the reactant- and transition-state energies in Figure 10 was recalculated after replacing H_2O and H_2O_2 with D_2O and D_2O_2, respectively. The isotopic substitution influences zero-point and vibrational energy levels in the reactant and transition states as well as tunneling probabilities. Computed tunneling corrections and apparent activation parameters are shown in Tables S7 and S8, respectively. As expected, the overall result of isotopic substitution is a slightly larger apparent activation barrier energy for each step, consistent with typical primary KIEs.[88]

The forward rate constants k_{1w} and k_{2w} are related to the directly calculated rate constants for the elementary steps (based on Figure 10) using the pseudo-steady-state approximations defined in eqs 19 and 20:

$$k_{1w} = \frac{k_{MTO\rightarrow I_1} k_{I_1\rightarrow A}}{k_{I_1\rightarrow MTO} + k_{I_1\rightarrow A}} \approx k_{MTO\rightarrow I_1} \quad (19)$$

$$k_{2w} = \frac{k_{A\rightarrow I_2} k_{I_2\rightarrow B}}{k_{I_2\rightarrow A} + k_{I_2\rightarrow B}} \approx k_{A\rightarrow I_2} \quad (20)$$

Both must be multiplied by the appropriate value of $[H_2O]^m$ (or $[D_2O]^m$) to obtain the pseudo-second-order rate constants k_1 and k_2. Fractionation factors were computed as $\phi_1^* = (k_1^D/k_1)^{1/(m+1)}$ and $\phi_2^* = (k_2^D/k_2)^{1/(m+1)}$, where m is the number of H_2O/D_2O molecules in the rate-determining transition state. Computed KIEs and fractionation factors for the $1H_2O/1D_2O$ and $2H_2O/2D_2O$ pathways, as well as with ensemble-averaged properties, are shown in Table 3. Computed and experimental rate constants are compared in Table S9.

The computed KIE for the formation of **A** from MTO via a $1H_2O$-assisted transition state, k_1/k_1^D = 6.1, is quite large compared to the experimental value, 3.8. In contrast, the computed KIE for the $1H_2O$-assisted formation of **B** from **A**,

Table 3. Comparison of Computed and Experimental KIEs for the Sequential Formation of Peroxo Complexes A and B from MTO, at 25.0 °C

	calculated[a]			experimental[b]	
parameter	$1H_2O/D_2O$	$2H_2O/D_2O$	ensemble	m = 1	m = 2
k_1/k_1^D	6.05	3.91	5.47	3.77	3.54
ϕ_1^*	0.406	0.635	0.567[c]	0.515	0.656
k_2/k_2^D	3.26	2.91	2.94	3.74	3.51
ϕ_2^*	0.554	0.700	0.698[c]	0.517	0.658

[a]Pseudo-second-order rate constants were calculated using the activation parameters in Tables 2 and S8. [b]Measured for $[H_2O + D_2O]$ = 3.1 M. The experimental KIEs differ slightly for curvefits involving m = 1 and m = 2 only because k_1^D and k_2^D are extrapolated to n = 1 for a chosen m. [c]Fractionation factors for the ensemble average were computed using m = 2, since this value resulted in the best fit to the experimental data.

DOI: 10.1021/jacs.5b03750
J. Am. Chem. Soc. 2015, 137, 9604−9616

k_2/k_2^D = 3.3, is slightly under-predicted compared to the experimental value, 3.7. In contrast, both computed KIEs involving the $2H_2O$-assisted transition states, k_1/k_1^D= 3.9 and k_2/k_2^D = 2.9, are in reasonable agreement with the corresponding experimental values (both 3.5, extrapolated using m = 2 as the best experimental fit). The large difference in computed KIEs (k_1/k_1^D vs k_2/k_2^D) for the $1H_2O$-assisted transition states, and between the $1H_2O$- and $2H_2O$-assisted transition states, was unexpected, since the structures of all transition states are similar. It stems from differences in tunneling prefactors, which result from differences in transition-state imaginary frequencies.

Subtle energetic differences between $1H_2O$- and $2H_2O$-assisted transition states make it difficult to identify the dominant pathway conclusively based solely on the computations, given the limited chemical accuracy of DFT calculations. Transition states containing both $1H_2O$ and $2H_2O$ molecules may both contribute to the observed KIEs. However, the calculated KIEs for the $2H_2O$-assisted pathways agree more closely with experiment than KIEs for the $1H_2O$-assisted pathway. This gives further weight to the hypothesis that the most favorable transition states involve two water molecules.

Scheme 3 shows the multiple roles of water in olefin epoxidation catalyzed by MTO, based on all of our experimental and computational findings. It defines our rate constant notation explicitly, and shows all transition states where water influences the reaction rates. We stress that both cycles contribute to epoxidation reactions although their relative rates depend on $[H_2O_2]/[Re]_T$, which varies as a function of conversion.

Relative Contributions of Water on the Overall Epoxidation Rate. To explore the precise effects of the various types of water acceleration on the rates of cyclohexene epoxidation seen in Figure 1, we simulated the catalytic process numerically, using the rate expressions in eqs 6−10. Pseudo-steady-state solutions were also computed, for comparison with the numerical simulations. For comparison with experiments, equilibria involving the peroxorhenium complexes were established first, prior to the onset of cyclohexene epoxidation. To model the water dependence of the ligand-exchange reactions, k_1, k_{-1}, and k_2 were assumed to depend on $[H_2O]^2$, while k_{-2} was assumed to depend on $[H_2O]$, consistent with detailed balance. The qualitative conclusions drawn from this analysis are not sensitive to the precise order m of the dependence on $[H_2O]^m$ for the ligand-exchange steps. The rate constants k_{3app} and k_{4app} for the epoxidation steps were extrapolated from Figure 2, using eqs 14 and 15 to adjust for their water dependence.

Figure 12 shows cyclohexene conversion and Re speciation profiles simulated under $[H_2O_2]$-limited conditions (corresponding to the experimental conditions in Figure 1a). Water acceleration is clearly evident, and the agreement with experiments is excellent, Figure S2. Because the catalyst concentration is small compared to $[H_2O_2]$, the pseudo-steady-state solutions agree well with the numerical solutions, with the exception of the transient mismatch expected at very early times.[51] MTO-catalyzed epoxidations at low water concentrations are predicted to be extremely slow. Under anhydrous conditions, the rates for the unassisted mechanism would be 5 orders of magnitude slower than those measured in 0.2 M H_2O, implying that such reactions in CH_3CN are undoubtedly catalyzed by adventitious water. Nevertheless, appreciable epoxidation rates under anhydrous conditions can

Scheme 3. Principal Species Proposed to Be Involved in the Catalytic Cycle during Olefin Epoxidation by MTO, Highlighting the Role of Water and Showing the Corresponding Rate Constants, Based on Combined Experimental/Computational Analysis[a]

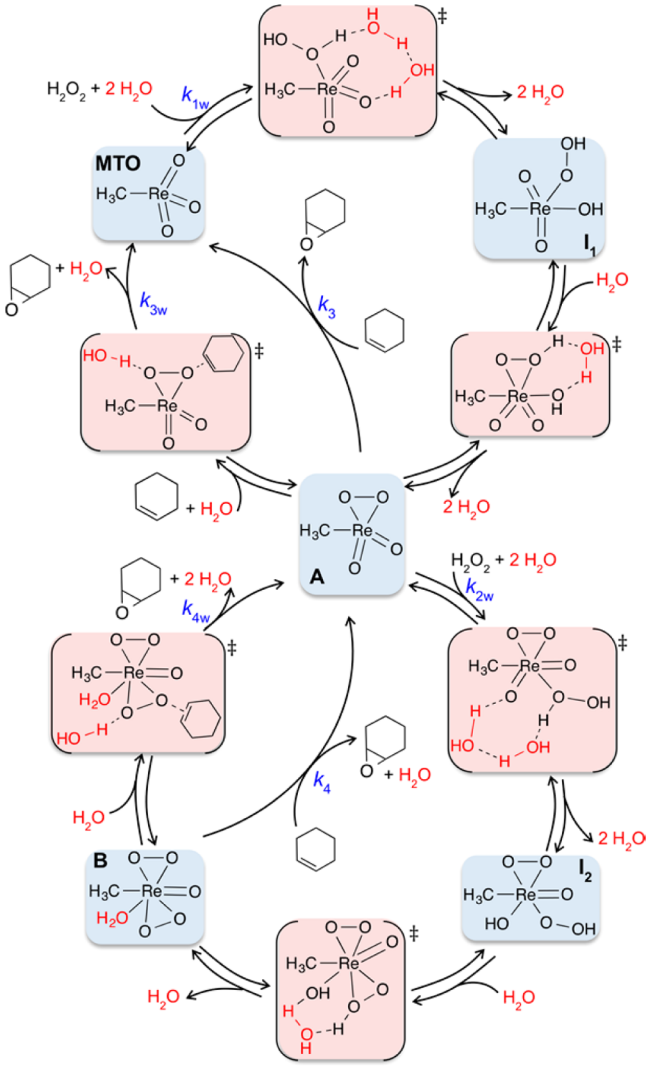

[a]The number of water molecules, m, that participate in each transition state can vary; the structures shown here are the most probable numbers in aqueous CH_3CN containing 2 M H_2O. Transition states are highlighted in red; stable species are highlighted in blue. The relative turnover frequencies of the two coupled catalytic cycles depend strongly on the reaction conditions.

be obtained with the addition of pyridine bases.[89,90] Interestingly, the accelerating effect of pyridine bases is inhibited by the presence of water.[90]

While essentially all Re is present as **B** prior to initiation of the reaction by addition of cyclohexene, Figure 12b shows that it is mostly converted to **A** and MTO shortly after the reaction starts. Although $[H_2O_2] \gg [Re]_T$ for most of the reaction, the fraction of Re existing as **B**, α_B, remains very low throughout (<5%), and **B** is responsible for <7% of epoxidation with excess cyclohexene for all water concentrations considered here. The value of α_{MTO} gradually increases as H_2O_2 is consumed. The effect of H_2O on Re speciation during epoxidation is simulated in Figure S3. Increasing $[H_2O]$ causes the ratio $[\mathbf{A}]/[MTO]$ to

DOI: 10.1021/jacs.5b03750
J. Am. Chem. Soc. 2015, 137, 9604−9616

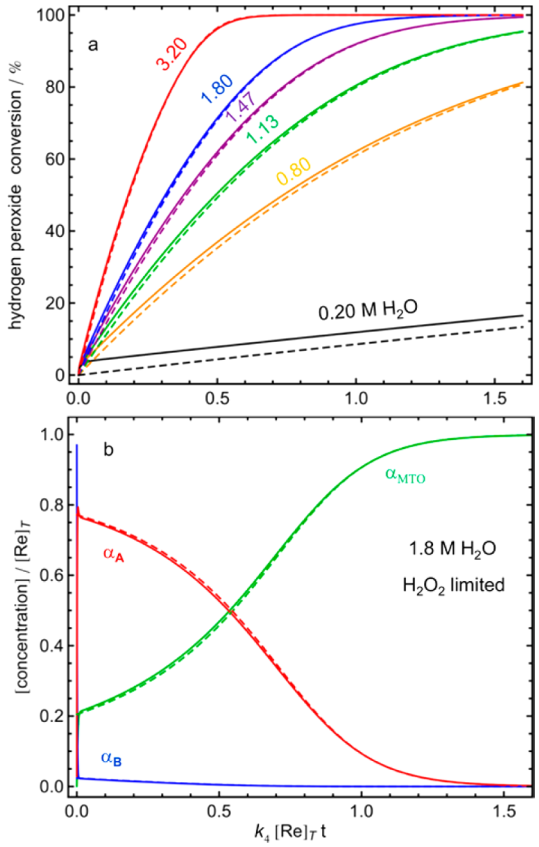

Figure 12. Simulated kinetic profiles for (a) the epoxidation of cyclohexene (2.0 M) by H_2O_2 (0.20 M) catalyzed by MTO (4.0 mM) in CH_3CN containing 0.20−3.2 M H_2O at 15.0 °C; and (b) Re speciation under the same reaction conditions and 1.8 M H_2O. Here k_4 is the water-independent rate constant for the epoxidation of cyclohexene by **B** (4.0×10^{-2} M^{-1} s^{-1}), $\alpha_A = [A]/[Re]_T$, $\alpha_B = [B]/[Re]_T$, $\alpha_{MTO} = [MTO]/[Re]_T$. The abscissa (time axis) has been nondimensionalized by $k_4[Re]_T$ so that the figures describe results for all Re concentrations. Solid lines indicate numerical solutions to eqs 6−10. Dashed lines show pseudo-steady-state solutions for [**A**], [**B**], and [MTO].

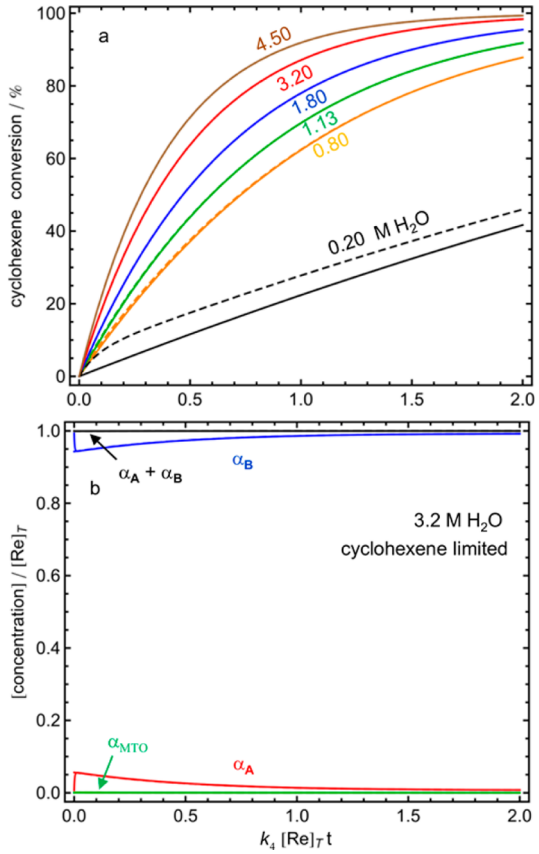

Figure 13. Simulated kinetic profiles for (a) the epoxidation of cyclohexene (20 mM) by H_2O_2 (0.50 M) catalyzed by MTO (2.0 mM) in CH_3CN containing 0.10−4.5 M H_2O at 15.0 °C; and (b) Re speciation under the same reaction conditions and 3.2 M H_2O. Here k_4 is the water-independent rate constant for the epoxidation of cyclohexene by **B** (4.0×10^{-2} M^{-1} s^{-1}), $\alpha_A = [A]/[Re]_T$, $\alpha_B = [B]/[Re]_T$, $\alpha_{MTO} = [MTO]/[Re]_T$. The abscissa (time axis) has been nondimensionalized by $k_4[Re]_T$ so that the figures describe results for all Re concentrations. Solid lines indicate numerical solutions to eqs 6−10. Dashed lines show pseudo-steady-state solutions for [**A**], [**B**], and [MTO]. (The dashed lines are not visible in (b), since the agreement with the numerical solutions is very good.)

increase, effectively accelerating the epoxidation rate because more of the active species is present. For $[H_2O] > 0.80$ M, water catalyzes the conversion of MTO to **A** slightly faster than cyclohexene is epoxidized by **A**.

Figure 13 shows simulated kinetic profiles under [cyclohexene]-limited conditions (corresponding to the experimental conditions in Figure 1b). Again, the pseudo-steady-state solutions agree well with the numerical solutions because the concentration of catalyst is much smaller than that of cyclohexene. Here too, water catalyzes the overall epoxidation reaction, but for a different reason. Essentially all Re exists as **B** prior to initiation of the reaction by addition of cyclohexene, Figure 13b (shown for 3.2 M H_2O). A significant amount is converted to **A** soon after the reaction starts. The sum [**A**] + [**B**] remains nearly constant, while [MTO] is negligible. Thus, water acceleration does not arise due to faster conversion of MTO to **A**. Instead, increasing $[H_2O]$ causes the abundance of **B** to increase relative to **A**, Figure S4. Both experimental measurements and computational predictions of the activation free energies (Table 1) suggest that **B** is more reactive than **A** toward cyclohexene. Thus, the rate of epoxidation accelerates as $[H_2O]$ increases, simply because the ratio [**B**]/[**A**] increases. The rate of formation of **B** from **A** becomes slightly larger than the rate of epoxidation by **B** as the reaction progresses or when the water concentration increases, Figure S4. Interestingly, the simulated water acceleration effect is less pronounced as the water concentration continues to increase, similar to observations in Figure 1b, because **B** is already by far the dominant species at $[H_2O] = 3.0$ M.

■ CONCLUSIONS

Water that is present either as a cosolvent or as a reaction product can have an easily overlooked but important mechanistic role in homogeneous catalytic processes. Our understanding of water-accelerated organic reactions as well as transition metal-catalyzed reactions in which the solvent acts as a co-catalyst is hampered by the complexity of condensed phases and the multiple ways in which water can participate in transition states. MTO-catalyzed epoxidation by H_2O_2 shows strong nonlinear water acceleration effects, even though no step in the catalytic cycle explicitly requires water as a reactant. The individual epoxidation steps involving the catalytically active peroxo complexes $CH_3ReO_2(\eta^2\text{-}O_2)$, **A**, and $CH_3ReO(\eta^2$-

DOI: 10.1021/jacs.5b03750
J. Am. Chem. Soc. 2015, 137, 9604−9616

$O_2)_2(H_2O)$, **B**, are weakly accelerated by water. Our computational results show that water lowers epoxidation barriers slightly when it forms a hydrogen bond to the spectator oxygen of a peroxo ligand in **A** and **B**. The primary effect of water on catalytic epoxidation arises from its acceleration of proton transfer from coordinated H_2O_2 to oxo ligands of MTO and **A** and to the hydroxo ligands of the corresponding η^1-hydroperoxo intermediates. Proton inventory experiments suggest that, on average, two water molecules participate directly in the rate-determining proton transfers. Ab initio free energy calculations including tunneling corrections and a thermodynamically consistent mixture of water hydration states support this conclusion by predicting activation parameters as well as fractionation factors for $2H_2O$-assisted transition states in reasonable agreement with experimentally obtained values.

Kinetic simulations confirm that water acceleration of catalytic epoxidation arises primarily from $[H_2O]$-catalyzed formation of the active peroxo species, altering the Re speciation. The reaction rate in CH_3CN is predicted to be vanishingly slow in the absence of water, and even reactions conducted under nominally anhydrous conditions are likely promoted by catalytic amounts of adventitious water (and autocatalysis by the water produced in the epoxidation reaction). Strong water dependence is anticipated for other MTO-catalyzed oxidations where the key water-dependent steps involve peroxo complex formation.[91]

■ ASSOCIATED CONTENT

Supporting Information

Individual contributions to the total free energies of ground states, water-free, and water-assisted (D_2O-assisted) transition states; imaginary frequencies and tunneling corrections; computed rate constants; energies and Cartesian coordinates of all computed structures; a description of the microsolvation model and the proton inventory method; and full ref 52. The Supporting Information is available free of charge on the ACS Publications website at DOI: 10.1021/jacs.5b03750.

■ AUTHOR INFORMATION

Corresponding Authors

*baronp@engineering.ucsb.edu
*sscott@engineering.ucsb.edu

Author Contributions

#These authors contributed equally.

Notes

The authors declare no competing financial interest.

■ ACKNOWLEDGMENTS

B.R.G. acknowledges the PIRE-ECCI program (NSF-OISE 0530268) for a graduate fellowship. T.H. is grateful to Air Products for a graduate fellowship. This work was funded by the Catalysis Science Initiative of the U.S. Department of Energy, Basic Energy Sciences (DE-FG02−03ER15467).

■ REFERENCES

(1) Herrmann, W. A.; Wang, M. *Angew. Chem., Int. Ed. Engl.* **1991**, *30*, 1641−1643.
(2) Herrmann, W. A.; Fischer, R. W.; Rauch, M. U.; Scherer, W. *J. Mol. Catal.* **1994**, *86*, 243−266.
(3) Wang, W. D.; Espenson, J. H. *J. Am. Chem. Soc.* **1998**, *120*, 11335−11341.
(4) Espenson, J. H. *Chem. Commun.* **1999**, 479−488.
(5) Kühn, F. E.; Scherbaum, A.; Herrmann, W. A. *J. Organomet. Chem.* **2004**, *689*, 4149−4164.
(6) Hansen, P. J.; Espenson, J. H. *Inorg. Chem.* **1995**, *34*, 5839−5844.
(7) Al-Ajlouni, A. M.; Espenson, J. H. *J. Am. Chem. Soc.* **1995**, *117*, 9243−9250.
(8) Yamazaki, S.; Espenson, J. H.; Huston, P. *Inorg. Chem.* **1993**, *32*, 4683−4687.
(9) Al-Ajlouni, A. M.; Espenson, J. H. *J. Org. Chem.* **1996**, *61*, 3969−3976.
(10) Owens, G. S.; Durazo, A.; Abu-Omar, M. M. *Chem. - Eur. J.* **2002**, *8*, 3053−3059.
(11) Crucianelli, M.; Saladino, R.; De Angelis, F. *ChemSusChem* **2010**, *3*, 524−540.
(12) Butler, R. N.; Coyne, A. G. *Chem. Rev.* **2010**, *110*, 6302−6337.
(13) Gallezot, P. *Chem. Soc. Rev.* **2012**, *41*, 1538−1558.
(14) Besson, M.; Gallezot, P.; Pinel, C. *Chem. Rev.* **2014**, *114*, 1827−1870.
(15) Breslow, R. *Acc. Chem. Res.* **1991**, *24*, 159−164.
(16) Narayan, S.; Muldoon, J.; Finn, M. G.; Fokin, V. V.; Kolb, H. C.; Sharpless, K. B. *Angew. Chem., Int. Ed.* **2005**, *44*, 3275−3279.
(17) Saavedra, J.; Doan, H. A.; Pursell, C. J.; Grabow, L. C.; Chandler, B. D. *Science* **2014**, *345*, 1599−1602.
(18) Daté, M.; Okumura, M.; Tsubota, S.; Haruta, M. *Angew. Chem., Int. Ed.* **2004**, *43*, 2129−2132.
(19) Rozanska, X.; van Santen, R. A. In *Handbook of Zeolite Science and Technology*; Auerbach, S. M., Carrado, K. A., Dutta, P. K., Eds.; Dekker: New York, 2003; p 1000−1058.
(20) Ohnishi, Y.-Y.; Nakao, Y.; Sato, H.; Sakaki, S. *Organometallics* **2006**, *25*, 3352−3363.
(21) Kamata, K.; Hirano, T.; Kuzuya, S.; Mizuno, N. *J. Am. Chem. Soc.* **2009**, *131*, 6997−7004.
(22) Jee, J.-E.; Comas-Vives, A.; Dinoi, C.; Ujaque, G.; van Eldik, R.; Lledós, A.; Poli, R. *Inorg. Chem.* **2007**, *46*, 4103−4113.
(23) Dinoi, C.; Ciclosi, M.; Manoury, E.; Maron, L.; Perrin, L.; Poli, R. *Chem. - Eur. J.* **2010**, *16*, 9572−9584.
(24) Comas-Vives, A.; Lledós, A.; Poli, R. *Chem. - Eur. J.* **2010**, *16*, 2147−2158.
(25) Wahlen, J.; De Vos, D. E.; Jacobs, P. A. *Org. Lett.* **2003**, *5*, 1777−1780.
(26) Neimann, K.; Neumann, R. *Org. Lett.* **2000**, *2*, 2861−2863.
(27) Wurst, J. M.; Liu, G.; Tan, D. S. *J. Am. Chem. Soc.* **2011**, *133*, 7916−7925.
(28) Mountain, R. D. *J. Phys. Chem. B* **2010**, *114*, 16460−16464.
(29) French, H. T. *J. Chem. Thermodyn.* **1987**, *19*, 1155−1161.
(30) Wakisaka, A.; Abdoul-Carime, H.; Yamamoto, Y.; Kiyozumi, Y. *J. Chem. Soc., Faraday Trans.* **1998**, *94*, 369−374.
(31) Pestovsky, O.; van Eldik, R.; Huston, P.; Espenson, J. H. *J. Chem. Soc., Dalton Trans.* **1995**, 133−137.
(32) Gonzales, J. M.; Distasio, R., Jr.; Periana, R. A.; Goddard, W. A., III; Oxgaard, J. *J. Am. Chem. Soc.* **2007**, *129*, 15794−15804.
(33) Wang, W. D.; Espenson, J. H. *Inorg. Chem.* **1997**, *36*, 5069−5075.
(34) Hwang, T.; Goldsmith, B. R.; Peters, B.; Scott, S. L. *Inorg. Chem.* **2013**, *52*, 13904−13917.
(35) Hu, H.; Yang, W. *Annu. Rev. Phys. Chem.* **2008**, *59*, 573−601.
(36) Dutta Banik, S.; Chandra, A. *J. Phys. Chem. B* **2014**, *118*, 11077−11089.
(37) Morokuma, K. *Bull. Korean Chem. Soc.* **2003**, *24*, 797−801.
(38) Chandrasekhar, J.; Smith, S. F.; Jorgensen, W. L. *J. Am. Chem. Soc.* **1984**, *106*, 3049−3050.
(39) Chandrasekhar, J.; Smith, S. F.; Jorgensen, W. L. *J. Am. Chem. Soc.* **1985**, *107*, 154−163.
(40) Tomasi, J.; Mennucci, B.; Cammi, R. *Chem. Rev.* **2005**, *105*, 2999−3094.
(41) Takano, Y.; Houk, K. N. *J. Chem. Theory Comput.* **2005**, *1*, 70−77.
(42) Katari, M.; Rajaraman, G.; Ghosh, P. *J. Organomet. Chem.* **2015**, *775*, 109−116.

DOI: 10.1021/jacs.5b03750
J. Am. Chem. Soc. 2015, 137, 9604−9616

(43) Gisdakis, P.; Antonczak, S.; Köstlmeier, S.; Herrmann, W. A.; Rösch, N. *Angew. Chem., Int. Ed.* **1998**, *37*, 2211−2214.
(44) Di Valentin, C.; Gandolfi, R.; Gisdakis, P.; Rösch, N. *J. Am. Chem. Soc.* **2001**, *123*, 2365−2376.
(45) Kuznetsov, M. L.; Pombeiro, A. J. L. *Inorg. Chem.* **2009**, *48*, 307−318.
(46) Karlsson, E. A.; Privalov, T. *Chem. - Eur. J.* **2009**, *15*, 1862−1869.
(47) Herrmann, W. A.; Fischer, R. W.; Marz, D. W. *Angew. Chem., Int. Ed. Engl.* **1991**, *30*, 1638−1641.
(48) Yudin, A. K.; Sharpless, K. B. *J. Am. Chem. Soc.* **1997**, *119*, 11536−11537.
(49) Altmann, P.; Cokoja, M.; Kühn, F. E. *Eur. J. Inorg. Chem.* **2012**, *2012*, 3235−3239.
(50) *Mathematica*, Version 9.0: Wolfram Research Inc.: Champaign, IL, 2012.
(51) Heineken, F. G.; Tsuchiya, H. M.; Aris, R. *Math. Biosci.* **1967**, *1*, 95−113.
(52) Frisch, M. J.; Trucks, G. W.; Schlegel, H. B. et al. *Gaussian 09*, Revision C.01, Gaussian, Inc.: Wallingford, CT, 2009.
(53) Chai, J.-D.; Head-Gordon, M. *Phys. Chem. Chem. Phys.* **2008**, *10*, 6615−6620.
(54) Roy, L. E.; Hay, P. J.; Martin, R. L. *J. Chem. Theory Comput.* **2008**, *4*, 1029−1031.
(55) Figgen, D.; Peterson, K. A.; Dolg, M.; Stoll, H. *J. Chem. Phys.* **2009**, *130*, 164108.
(56) Barone, V.; Cossi, M. *J. Phys. Chem. A* **1998**, *102*, 1995−2001.
(57) Cossi, M.; Rega, N.; Scalmani, G.; Barone, V. *J. Comput. Chem.* **2003**, *24*, 669−681.
(58) McQuarrie, D. A. *Statistical Mechanics*; University Science Books: Sausalito, CA, 2000.
(59) Pliego, J. R.; Riveros, J. M. *J. Phys. Chem. A* **2001**, *105*, 7241−7247.
(60) Sicinska, D.; Paneth, P.; Truhlar, D. G. *J. Phys. Chem. B* **2002**, *106*, 2708−2713.
(61) da Silva, E. F.; Svendsen, H. F.; Merz, K. M. *J. Phys. Chem. A* **2009**, *113*, 6404−6409.
(62) Ibarguen, C.; Manrique-Moreno, M.; Hadad, C. Z.; David, J.; Restrepo, A. *Phys. Chem. Chem. Phys.* **2013**, *15*, 3203−3211.
(63) Peters, B.; Trout, B. L. *Biochemistry* **2006**, *45*, 5384−5392.
(64) Eyring, H. *J. Chem. Phys.* **1935**, *3*, 107.
(65) Skodje, R. T.; Truhlar, D. G.; Garrett, B. C. *J. Chem. Phys.* **1982**, *77*, 5955−5976.
(66) Fermann, J. T.; Auerbach, S. *J. Chem. Phys.* **2000**, *112*, 6787−6794.
(67) Zhu, Z.; Espenson, J. H. *J. Org. Chem.* **1995**, *60*, 1326−1332.
(68) Mountain, R. D. *J. Phys. Chem. A* **1999**, *103*, 10744−10748.
(69) Frasson, C. M. L.; Brandão, T. A. S.; Zucco, C.; Nome, F. *J. Phys. Org. Chem.* **2006**, *19*, 143−147.
(70) Frasson, C. M. L.; Brandão, T. A. S.; Zucco, C.; Nome, F. *J. Phys. Org. Chem.* **2006**, *19*, 143.
(71) Oldiges, C.; Wittler, K.; Tönsing, T.; Alijah, A. *J. Phys. Chem. A* **2002**, *106*, 7147−7154.
(72) Venkatasubban, K. S.; Schowen, R. L. *Crit. Rev. Biochem. Mol. Biol.* **1984**, *17*, 1−44.
(73) Krishtalik, L. I. *Mendeleev Commun.* **1993**, *3*, 66−67.
(74) Schowen, K. B. J. *Transition States of Biochemical Processes*; Plenum Press: New York, 1978.
(75) Orr, W. J. C.; Butler, J. A. V. *J. Chem. Soc.* **1937**, 330−335.
(76) Venkatasubban, K. S.; Bush, M.; Ross, E.; Schultz, M.; Garza, O. *J. Org. Chem.* **1998**, *63*, 6115−6118.
(77) Geissler, P. L.; Dellago, C.; Chandler, D.; Hutter, J.; Parrinello, M. *Science* **2001**, *291*, 2121−2124.
(78) Abu-Omar, M. M.; Hansen, P. J.; Espenson, J. H. *J. Am. Chem. Soc.* **1996**, *118*, 4966−4974.
(79) Wu, Y.-D.; Sun, J. *J. Org. Chem.* **1998**, *63*, 1752−1753.
(80) Sun, Y.; Chen, H. *J. Chem. Theory Comput.* **2014**, *10*, 579−588.
(81) Fukui, K. *Acc. Chem. Res.* **1981**, *14*, 363−368.
(82) Hratchian, H. P.; Schlegel, H. B. In *Theory and Applications of Computational Chemistry: The First 40 Years*; Dykstra, C. E., Frenking, G., Kim, K. S., Scuseria, G., Eds.; Elsevier: Amsterdam, The Netherlands, 2005; Vol. *1*, pp 195−249.
(83) Gandour, R. D. *Tetrahedron Lett.* **1974**, *15*, 295−298.
(84) Yang, K.; Zheng, J.; Zhao, Y.; Truhlar, D. G. *J. Chem. Phys.* **2010**, *132*, 164117−164110.
(85) Zhao, Y.; Truhlar, D. G. *J. Chem. Theory Comput.* **2011**, *7*, 669−676.
(86) Schenker, S.; Schneider, C.; Tsogoeva, S. B.; Clark, T. *J. Chem. Theory Comput.* **2011**, *7*, 3586−3595.
(87) Yates, K.; Modro, T. A. *Acc. Chem. Res.* **1978**, *11*, 190−196.
(88) Westheimer, F. H. *Chem. Rev.* **1961**, *61*, 265−273.
(89) Rudolph, J.; Reddy, K. L.; Chiang, J. P.; Sharpless, K. B. *J. Am. Chem. Soc.* **1997**, *119*, 6189−6190.
(90) Wang, W.-D.; Espenson, J. H. *J. Am. Chem. Soc.* **1998**, *120*, 11335−11341.
(91) Romão, C. C.; Kühn, F. E.; Herrmann, W. A. *Chem. Rev.* **1997**, *97*, 3197−3246.

DOI: 10.1021/jacs.5b03750
J. Am. Chem. Soc. 2015, 137, 9604−9616